Interaction of Coinage Metal Clusters with Chalcogen Dihydrides

A.H. Pakiari* and Z. Jamshidi†

Chemistry Department, College of Sciences, Shiraz University, Shiraz 71454, Iran

Received: May 07, 2008; Revised Manuscript Received: June 23, 2008

The interaction of chalcogen dihydrides (H_2E; E = O, S, and Se) with small coinage metal clusters (M_n; M = Cu, Ag, and Au, n = 3 and 4) is studied based on density functional theory, with a focus on the nature of chalcogen−metal bonds. A newly developed pseudopotential-based correlation-consistent basis set is used for metal clusters together with the 6-311++G** basis set for the remaining atoms. Geometrical data identified that no significant deviation has been observed for molecules before and after complexation. For these three metals, binding energy calculations indicate that gold has the highest and silver has the lowest affinities for interaction with H_2E. In comparison with gold and copper, complexation between silver and chalcogen dihydrides is significantly weaker. It is found that interaction of H_2E molecules with the coinage metals have the order of $H_2Se > H_2S > H_2O$. Therefore, in agreement with experimental works, our calculations confirm that the gold−selenium bond is the most stable. The nature of M−E bonds is also interpreted by means of the quantum theory of atoms in molecules (QTAIM) and natural bond orbital (NBO) analyses. According to the QTAIM results, the bonds are found to be partially ionic and partially covalent. Natural resonance theory (NRT) is used to calculate natural bond order and bond polarity. The NRT result indicates that the percentage of polarity of M−E bonds is affected by coinage metals.

1. Introduction

Nanocluster coinage metals and compounds have attracted attention in the areas of medicine, catalysis, fabrication of nanodevices, and other applications due to their unique physical and chemical properties[1,2] which depend strongly on cluster size. The shape and size of coinage nanoparticles play an important role in determining their chemical reactivity.[3]

In the past few years, atomic and molecular chemisorptions on small coinage metal clusters, especially gold, have received considerable attention, both experimentally and theoretically.[4] Molecules containing sulfur atoms often form particularly stable gold nanoclusters due to the strength of the gold−sulfur bond.[5] The gold−sulfur bond is extremely important in the formation of self-assembled monolayers,[6] single-molecule devices,[7] and markers of biological molecules, such as DNA and proteins. [8] Several theoretical investigations describing the adsorption of alkane thiols on a gold surface have been represented by cluster models.[9] In the development of single-molecule devices, one of the points to be considered is to have highly stable metal−molecule junctions.[10] To find a substitute for the gold−sulfur bond, the most promising way involves the use of other chalcogen compounds. Taniguchi et al.[11] have performed photoelectron spectroscopy (X-ray and UV photoemission spectroscopy) to investigate the bonding condition between gold and chalcogen atoms by employing benzenethiol, benzeneselenol, and biphenyl ditellurid. They clarified that a gold−selenium bond is more suitable for molecular electronics than the other bonds.

Besides gold, the interactions of molecules with copper and silver and binary gold−silver clusters/nanoparticles have also drawn remarkable attention.[12] However, in distinct contrast to gold, comparatively little work has been done on interactions of chalcogen molecules with other coinage metals.[13] Copper is especially interesting as a much cheaper substitute for gold; available experimental evidence suggests that substitution of Au by Cu also modifies the underlying chemistry at the metal−molecule junction.[14] Silver has the same electronic configuration as gold and copper; therefore, it is natural to anticipate similar properties. On the other hand, theoretical and experimental studies have shown that the interaction of molecules with silver atoms and clusters is significantly weaker than that with the other two metal clusters.[15]

To design new molecular devices, it is extremely important to analyze the chemical interactions of molecular systems at the junctions. Therefore, in the present work, we focused on the interactions between chalcogens and three coinage metals, gold, silver, and copper. Interactions of chalcogen dihydrides (H_2E; E = O, S, and Se) with coinage nanoclusters (M_3 and M_4; M = Cu, Ag, and Au) are studied theoretically, and the structural, electronic, and bonding properties of these complexes are considered.

2. Computational Details

Geometries of H_2E (E = O, S, and Se) molecules and complexes with coinage metal clusters M_3 and M_4 (M = Cu, Ag, and Au) were fully optimized using density functional theory (DFT) with the B3LYP functional[16] by the Gaussian 03 suite of programs.[17] Recently developed pseudopotential-based augmented correlation-consistent basis sets,[18] aug-cc-pVDZ-PP and aug-cc-pVTZ-PP based on the small core relativistic PPs of Figgen et al.,[19] were employed for coinage metals, while for H_2E molecules, the 6-311++G** basis set was used. In order to compare the results of the aug-cc-pVDZ-PP basis set with those of the aug-cc-pVTZ-PP, a set of calculations has been carried out for Au_3-EH_2 complexes. The comparison covered all geometrical parameters, vibrational frequencies, and binding energies; almost all relative differences were less than 2.0%. Thus, compared with the aug-cc-pVDZ-PP basis, the aug-cc-

* To whom correspondence should be addressed. E-mail: pakiari@susc.ac.ir.

† E-mail: na.jamshidi@gmail.com.

10.1021/jp804033w CCC: $40.75
Published on Web 08/07/2008

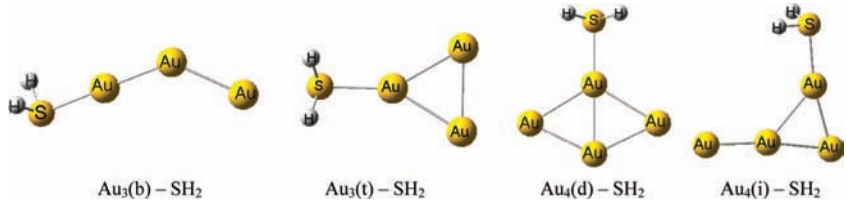

Figure 1. Optimized geometry of Au_n-SH_2 complexes.

pVTZ-PP basis set does not significantly improve calculated results, and consequently, only the aug-cc-pVDZ-PP basis set was used for the remaining molecules.

The harmonic vibrational frequencies and the corresponding zero-point vibrational energies (ZPVE) were calculated in all of the optimized geometries, and real frequencies were obtained in all of the cases. The binding energy ΔE_b of the complex M_n-EH_2 is defined in a standard way as the absolute value of the energy difference $\Delta E_b = E_{M_n-EH_2} - (E_{M_n} + E_{H_2E})$, and its ZPVE-corrected values are reported throughout this work.

To reveal the nature of bonds, the NBO and QTAIM analyses were used. The NBO analysis introduced by Weinhold and coworkers[20] transforms the delocalized molecular orbitals into localized ones that are closely tied to chemical bond concepts. We paid particular attention to natural population analysis (NPA) charges[21] and charge transfers, natural bond orders, and bond polarities which can be predicted by natural resonance theory (NRT).[22−24] In addition, the topological features of the electron density, $\rho(r)$, and its Laplacian, $\nabla^2\rho(r)$, at bond critical points (BCPs) were computed based on Bader's QTAIM.[25] The GENNBO[26] and AIM2000[27] programs were used to calculate NRT and QTAIM properties, respectively.

3. Result and Discussion

3.1. Structure and Energetics of Free Clusters. Physical and chemical properties of coinage metal clusters depend strongly on cluster size; small clusters are more reactive than bulk materials.[3] Gold clusters favoring 2D structures are very common building "bricks" for nanostructured materials. Moreover, the trimers are known to play a special role in coinage metal halides in the gas phase, and there is an unusual abundance of trimers in their vapor.[28−30]

Determining minimum-energy structures for trimers and tetramers of coinage metal clusters is difficult due to low-lying isomers. For the M_3 clusters, we have found the minimum-energy structure to be bent with C_{2v} symmetry, which is shown by M_3(b) in Figure 1, with obtuse angles of 133.80, 139.15, and 117.74° and M−M bond lengths of 2.596, 2.655, and 2.310 Å for gold, silver, and copper clusters, respectively. These values are in agreement with the results reported in ref 31. For M_3, there is also another low-lying isomer with D_{3h} symmetry, M_3(t) (Figure 1). For neutral coinage metal clusters, the energy difference between the triangular (D_{3h}) and linear-like structures (C_{2v}) is very small.

For M_4 clusters, we have found the minimum-energy structure to be diamond-shaped with D_{2h} symmetry.[31] There is also another isomer (which has a "dangling" M atom bonded to a M_3 group) with C_{2v} symmetry which is 0.04 eV lower in energy for gold and 0.12 and 0.27 eV higher for silver and copper, respectively. We denote the diamond-shaped structures by M_4(d) and the isomeric structure by M_4(i) (Figure 1).

3.2. Structure and Energetics of M_n-EH_2 (n = 3, 4; E = O, S, Se) Complexes. In order to test the performance of the computational method employed in the present investigation, we did the calculation for $M-SH_2$ (M = Cu, Ag, and Au) complexes and compared our results with spin-adapted ROHF CCSD(T) calculation by Urban et al.[32] For $Cu-SH_2$, $Ag-SH_2$, and $Au-SH_2$ complexes, B3LYP results for binding energies are −5.95, −1.88, and −8.18 mHartree, which are found to be in good agreement with ROHF CCSD(T) values, −5.99, −1.99, and −9.08 mHartree, respectively.

TABLE 1: Geometrical Features and Binding Energies of Au_n-EH_2 Complexes

complex	r(Au−E)[a][b]	Δr(E−H)[c]	Δ(∠HEH)[d]	υ(Au−E)[e]	ΔE_b[f]
Au_3(b)−OH_2	2.348	0.003	1.46	235.36	−8.15
Au_3(b)−SH_2	2.444	0.004	0.52	212.57	−15.12
Au_3(b)−SeH_2	2.536	0.002	0.07	181.14	−17.22
Au_3(t)−OH_2	2.316	0.003	1.64	248.62	−8.39
Au_3(t)−SH_2	2.398	0.005	0.37	236.64	−17.06
Au_3(t)−SeH_2	2.495	0.006	−0.12	186.36	−19.47
Au_4(d)−OH_2	2.333	0.002	1.73	245.49	−9.84
Au_4(d)−-SH_2	2.406	0.004	0.55	233.61	−18.76
Au_4(d)−SeH_2	2.501	0.004	0.02	184.57	−21.15
Au_4(i)−OH_2	2.307	0.003	1.22	262.14	−12.30
Au_4(i)−SH_2	2.412	0.004	0.58	235.10	−20.57
Au_4(i)−SeH_2	2.508	0.005	0.11	190.86	−22.64

[a] E is O, S, or Se. [b] The length of anchoring bonds, in Å. [c] The difference between bond lengths of E−H in the complexed and isolated fragment, in Å. [d] The difference between the bond angle of ∠HEH in the complexed and isolated fragment, in degrees. [e] Vibrational frequency of anchoring bonds in the complex, in cm^{-1}. [f] The binding energy ΔE_b (including zero-point energy correction), in kcal mol^{-1}.

3.2.1. Complexes of Chalcogen Dihydrides with Gold Clusters. The results of calculations for Au_3 and Au_4 complexes with H_2E molecules are collected in Table 1; their important features are presented graphically in Figures 2 and 3. For all Au_n-EH_2 complexes, geometries of Au_n and H_2E molecules do not change significantly after interaction. Clearly in Table 1, for H_2E molecules in the complexes, there is hardly any deviation observed in ∠HEH angles and H−E bond lengths from isolated ones. This property of the H_2E molecule to retain its original geometry is important for applications of these clusters in nanodevices such as a sensor molecule in order to probe cluster properties.

For all Au_3-EH_2 complexes, the E atom is bonded to a single metal atom. From Au_3(b) to the Au_3(t) cluster, the bond lengths of Au−E decrease about 2.0%, and the binding energies and Au−E vibrational frequencies increase about 10.0 and 5.0%, respectively. For Au_4(d)−EH_2, the E atom is bonded to a Au atom on the shorter D_{2h} axis, while for Au_4(i)−EH_2, the E atom is bonded to a Au atom of the Au_3 group (not bonded to the dangling Au atoms). From Au_4(d) to Au_4(i) complexes, the Au−E bond length changes slightly, and the binding energy and Au−E vibrational frequency increase about 10.0 and 3.0%, respectively. Clearly in Figure 2, for Au−E bonds, the bond lengths and binding energies changed slightly for different gold cluster conformers.

In all of the Au_n-EH_2 complexes, from H_2O to H_2Se compounds, as it is clear in Figure 3, the binding energy increases. Binding energies have been found to be in the range of −8.0 to −12.0, −15.0 to −20.0, and −17.0 to −22.0 kcal

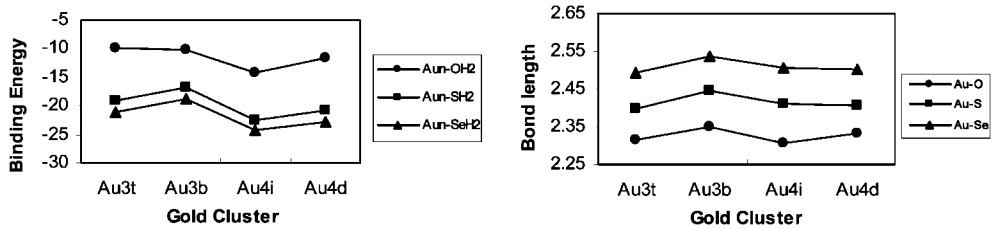

Figure 2. Binding energy (kcal mol^{-1}) and Au−E bond length (Å) curves as a function of different isomers of Au_3 and Au_4 clusters.

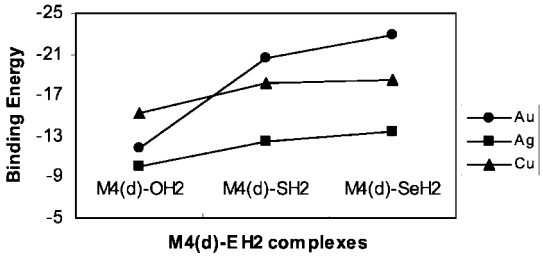

Figure 3. Binding energy (kcal mol^{-1}) for $M_4(d)-EH_2$ complexes, as a function of different chalcogen dihydrides.

mol^{-1} in Au_n-OH_2, Au_n-SH_2, and Au_n-SeH_2 complexes, respectively. The values for Au_n-SH_2 and Au_n-SeH_2 complexes are about 48.9% larger than those of Au_n-OH_2, while the difference between the binding energies of Au_n-SH_2 and Au_n-SeH_2 is about 11.1%. Therefore, gold−S(Se) bonds are good candidates for metal−molecule junctions, and we can substitute gold−S with gold−Se to get a highly stable junction.

3.2.2. Complexes of Chalcogen Dihydrides with Silver and Copper Clusters. Results of calculations for Ag_n and Cu_n clusters ($n = 3, 4$) and complexes with H_2E molecules are collected in Table 2; their important features are presented graphically in Figures 3 and 4. The E atom is bonded to a single Ag and Cu atom, and like Au_n-EH_2 complexes, there is no significant deviation observed in ∠HEH angles and the H−E bond lengths.

In different forms of M_n-EH_2 complexes, the binding energies increase by going from oxygen to selenium, but interestingly, for Cu and Ag complexes, they do not increase as dramatically as those for the Au-containing species (Figure 3). For silver complexes, the difference of binding energies between Ag_n-OH_2 and Ag_n-SH_2 complexes is ∼18.2%, and that between Ag_n-SH_2 and Ag_n-SeH_2 complexes is ∼10.5%. For copper complexes, the differences of binding energies between Cu_n-OH_2 and Cu_n-SH_2 and that between Cu_n-SH_2 and Cu_n-SeH_2 complexes are about 15.7 and 2.7%, respectively. We can conclude that gold clusters can separate different chalcogenide compounds from each other, while these separations are hardly possible for copper and silver clusters.

The changes in binding energies from copper to gold complexes (for E = S) are shown in Figure 4. It is clear that the Ag−E bonds have the lowest values, while Au−E bonds have the highest values. For example, for $M_4(d)-SH_2$ complexes, the binding energies for M = Cu, Ag, and Au are −16.42, −10.84, and −18.76 kcal mol^{-1}, respectively. This trend can also be observed in the differences of bond lengths and vibrational frequencies of M−E bonds. In $M_4(d)-SH_2$ complexes, the M−S bond lengths are 2.270, 2.572, and 2.406 Å, and the M−S vibrational frequencies are 287.14, 145.97, and 233.61 cm^{-1} for copper, silver, and gold complexes, respectively. For the other M_n-EH_2 complexes, we find the same trend; in comparison with Au−E and Cu−E bonds, the Ag−E bonds have the largest bond lengths, lowest vibrational frequencies, and lowest bonding energies.

Comparing copper with gold clusters, it has been shown that copper has the higher affinity to interaction with H_2O, but for the other chalcogenide, the interaction with gold is stronger than that with copper. In the $Au_3(t)-S(Se)H_2$ and $Au_4(d)-S(Se)H_2$ complexes, the binding energies are about 5.0 and 16.0% more than those of the $Cu_3(t)-S(Se)H_2$ and $Cu_4(d)-S(Se)H_2$ complexes, respectively. Therefore, obviously for these types of clusters, there is not a large difference in the interaction energy, and possibly, gold can be substituted by copper in some cases.

3.2.3. Trends in Bonding Energies in M_n-EH_2 Complexes. In the case of M_n-EH_2 complexes, interaction effects can be obtained by assuming certain charge transfers from the lone pair of E atoms to the coinage metal atom. According to the classical molecular orbital picture, the transfer of the electronic charge to the metal will depend on the ionization potential (IP) of the lone-pair electron in H_2E and electron affinity (EA) of the metal and also requires certain overlap between the lone-pair orbital of E and the electron-acceptor orbital of M.

From the binding energy calculations, we find that for the same metal, the interactions of chalcogen dihydrides have the order of $H_2Se > H_2S > H_2O$. By comparing the first (lone pair) IP of H_2E molecules, it can be interpreted that the IP of H_2Se[33] is 0.60 eV lower than that of H_2S,[34] and that for H_2S is 2.14 eV lower than that for H_2O.[35] This should facilitate the partial charge transfer toward the coinage metals.

Obviously, for H_2S and H_2Se molecules, the interaction with coinage metals has the order of Au > Cu > Ag. The difference between gold and silver interactions can be explained by relativistic effects. This effect on valence shell properties increases down a column of the periodic table roughly with Z^2, in which Z is the full nuclear charge. In a many-electron atom, the relativistic effect tends to contract and stabilize the s and p shells and expand and destabilize the d and f shells.[36] There also exists a relativistic bond length contraction; this contraction is able to pull in the Au−E bond lengths to lengths similar to or less than those of the corresponding Ag−E bonds.[37] The lanthanide contraction (the effect of filling the 4f shell on the subsequent 6s and 6p shells) works in the same direction as relativistic effects. It makes the gold atom have a very close covalent radius compared to that of the silver, but with a much larger nuclear charge. As mentioned above, the electron affinity of the metal is the driving force for efficient formation of the molecular orbital in the M−E region. The nonrelativistic EA values for Cu, Ag, and Au, are 1.165, 1.054, and 1.161 eV, respectively.[38] The relativistic DKH CCSD(T) results,[38] 1.236, 1.254, and 2.229 eV, respectively, agree reasonably well with the corresponding experimental data (1.226, 1.303, and 2.309 eV for Cu, Ag, and Au, respectively[39]). Clearly, the large relativistic enhancement of the gold electron affinity leads to much bigger binding energy. It is also worthwhile to note that for Ag and Cu, the relativistic effect did not have a major effect on the electron affinity, in agreement with the results of Urban et al.[32] They found that the relativistic treatment with in the scalar DKH approximation does not lead to major differences

TABLE 2: Geometrical Features and Binding Energies of Ag_n-EH_2 and Cu_n-EH_2 Complexes

complex	r(Ag(Cu)−E[a])[b]	Δr(E−H)[c]	$\Delta(\angle$HEH)[d]	υ(Ag(Cu)−E[e])	ΔE_b[f]
Ag_3(b)−OH_2	2.455	0.002	1.04	194.61	−5.16
Ag_3(b)−SH_2	2.689	0.002	0.51	132.76	−5.83
Ag_3(b)−SeH_2	2.746	0.002	0.23	80.49	−6.81
Ag_3(t)−OH_2	2.396	0.002	1.40	217.06	−7.18
Ag_3(t)−SH_2	2.590	0.002	0.61	188.35	−9.06
Ag_3(t)−SeH_2	2.659	0.002	0.15	178.15	−10.34
Ag_4(d)−OH_2	2.380	0.002	1.63	226.18	−8.48
Ag_4(d)−SH_2	2.572	0.001	0.73	145.97	−10.84
Ag_4(d)−SeH_2	2.645	0.002	0.24	185.58	−12.09
Ag_4(i)−OH_2	2.388	0.003	0.72	226.11	−9.17
Ag_4(i)−SH_2	2.601	0.003	0.49	197.60	−10.95
Ag_4(i)−SeH_2	2.675	0.002	0.14	109.14	−11.72
Cu_3(b)−OH_2	2.092	0.004	1.69	291.67	−9.32
Cu_3(b)−SH_2	2.329	0.004	0.62	259.45	−10.40
Cu_3(b)−SeH_2	2.439	0.004	0.24	249.35	−10.72
Cu_3(t)−OH_2	2.057	0.002	2.18	317.03	−14.94
Cu_3(t)−SH_2	2.269	0.005	0.48	283.89	−17.67
Cu_3(t)−SeH_2	2.377	0.006	−0.13	265.53	−18.16
Cu_4(d)−OH_2	2.062	0.002	2.38	318.92	−13.21
Cu_4(d)−SH_2	2.270	0.004	0.68	287.14	−16.42
Cu_4(d)−SeH_2	2.379	0.005	0.05	269.85	−16.87

[a] E is O, S, or Se. [b] The length of anchoring bonds, in Å. [c] The difference between bond lengths of E−H in the complexed and isolated fragment, in Å. [d] The difference between the bond angle of ∠HEH in the complexed and isolated fragment, in degrees. [e] Vibrational frequency of anchoring bonds in the complex, in cm^{-1}. [f] The binding energy ΔE_b (including zero-point energy correction), in kcal mol^{-1}.

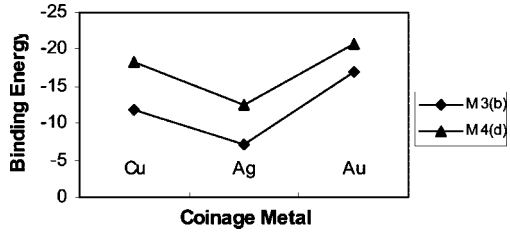

Figure 4. Binding energy (kcal mol^{-1}) for M_3(b)−SH_2 and M_4(d)−SH_2 complexes, as a function of different coinage metal cluster.

in the interaction energy of Ag and Cu atoms with H_2S. They obtained nonrelativistic and relativistic interaction energies for Cu−SH_2, −4.53 and −5.99 mHartree, respectively, and for Ag−SH_2, −1.53 and −1.99 mHartree, respectively. On the other hand, for Au−SH_2, nonrelativistic and relativistic interaction energies are −1.40 and −9.08 mHartree, respectively.

The difference in the Ag_n-EH_2 and Cu_n-EH_2 binding energies can be understood by the similar EA of these metals and shorter radius of copper. This permits a closer approach of Cu to E atoms and increases the overlap of the orbitals. In the nonrelativistic treatment, the increase of the effective radius of Ag and Au orbitals only weakens their interaction.

In the M_n-OH_2 complexes, the binding energies for copper are more than those for other coinage metals, and it is in agreement with the results of Urban et al.[13a] They claimed that a higher IP of H_2O hindered the charge-transfer bonding mechanism in these complexes, and in terms of binding energies, there is less similarity between M_n-OH_2 and $M_n-S(Se)H_2$ complexes.

3.3. Atoms-In-Molecules Analysis. In Bader's topological QTAIM analysis,[40] the nature of a bonding interaction is analyzed in terms of properties of the electron density and its derivatives. The Laplacian of $\rho(r)$ is related to the bond interaction energy by a local expression of the virial theorem.[25] A positive value of $\nabla^2\rho(r)$ at the bond critical point (BCP) shows a depletion of electronic charge along the bond. This is the case in a closed-shell electrostatic interaction. A negative value of $\nabla^2\rho(r)$, on the other hand, indicates that electronic charge is concentrated in the internuclear region. This is the case in an electron-sharing (or covalent) interaction.[25] A positive value of $\nabla^2\rho(r)$ at various BCPs of M−E bonds, in Table 3, indicates that these interactions are electrostatic in nature. The values of $\nabla^2\rho(r)$ for M−O bonds are about 30.0 and 47.0% more positive than the same value for M−S and M−Se bonds, respectively.

TABLE 3: Bond Critical Point Data (in au) from QTAIM Analysis

complex	BCP	ρ	$\nabla^2\rho(r)$	$G(r)$	$V(r)$	$H(r)$
Au_4(d)−OH_2	Au−O	0.0548	0.2506	0.0651	−0.0675	−0.0024
Au_4(d)−SH_2	Au−S	0.0853	0.1846	0.0703	−0.0945	−0.0241
Au_4(d)−SeH_2	Au−Se	0.0795	0.1363	0.0581	−0.0821	−0.0240
Au_4(i)−OH_2	Au−O	0.0577	0.2679	0.0702	−0.0734	−0.0032
Au_4(i)−SH_2	Au−S	0.0845	0.1803	0.0689	−0.0928	−0.0239
Au_4(i)−SeH_2	Au−Se	0.0789	0.1323	0.0569	−0.0807	−0.0238
Au_3(b)−OH_2	Au−O	0.0525	0.2394	0.0618	−0.0638	−0.0020
Au_3(b)−SH_2	Au−S	0.0787	0.1744	0.0643	−0.0850	−0.0207
Au_3(b)−SeH_2	Au−Se	0.0742	0.1312	0.0539	−0.0750	−0.0211
Au_3(t)−OH_2	Au−O	0.0561	0.2635	0.0685	−0.0711	−0.0026
Au_3(t)−SH_2	Au−S	0.0863	0.1896	0.0720	−0.0966	−0.0246
Au_3(t)−SeH_2	Au−Se	0.0804	0.1374	0.0589	−0.0834	0.0245
Ag_3(t)−OH_2	Ag−O	0.0406	0.1925	0.0482	−0.0483	−0.0001
Ag_3(t)−SH_2	Ag−S	0.0522	0.1336	0.0429	−0.0525	−0.0095
Ag_3(t)−SeH_2	Ag−Se	0.0522	0.1143	0.0396	−0.0506	−0.0110
Cu_3(t)−OH_2	Cu−O	0.0627	0.3450	0.0948	−0.1033	−0.0085
Cu_3(t)−SH_2	Cu−S	0.0746	0.1986	0.0724	−0.0951	−0.0227
Cu_3(t)−SeH_2	Cu−Se	0.0682	0.1530	0.0589	−0.0796	−0.0207

The electronic energy density $H(r)$ at a BCP is defined as $H(r) = G(r) + V(r)$, where $G(r)$ and $V(r)$correspond to the kinetic and potential energy densities at the BCPs, respectively.[41] The sign of $H(r)$ determines whether the accumulation of charge at a given point **r** is stabilizing ($H(r) < 0$) or destabilizing ($H(r) > 0$). The calculated values of $H(r)$ reported in Table 3 were found to be negative, which implies a stabilizing effect due to the amassing charge in the bonded region and the presence of a covalent bond. In Table 3, the calculated $H(r)$'s are negative for all M−E bonds. These values are more negative those for the M−S and M−Se bonds, the $H(r)$'s for these bonds are 85.0% more negative than the $H(r)$ for M−O bonds, indicating an increase in covalent character of M−S(Se) bonds compared

TABLE 4: Calculated NPA Charges of the Optimized Structures of M_n-EH_2 Complexes

complex	q_E	q_M	Δq_{ME}[a]	$\Delta q_{cluster}$[b]
$Au_3(t)-OH_2$	−0.926	0.258	1.184	−0.062
$Au_3(t)-SH_2$	−0.153	0.218	0.371	−0.166
$Au_3(t)-SeH_2$	0.020	0.189	0.209	−0.206
$Ag_3(t)-OH_2$	−0.941	0.264	1.205	−0.032
$Ag_3(t)-SH_2$	0.225	0.224	0.449	−0.091
$Ag_3(t)-SeH_2$	−0.116	0.210	0.326	−0.109
$Cu_3(t)-OH_2$	−0.952	0.320	1.272	−0.040
$Cu_3(t)-SH_2$	−0.229	0.265	0.494	−0.080
$Cu_3(t)-SeH_2$	−0.118	0.247	0.365	−0.090

[a] $\Delta q_{ME} = q_{M(complexed)} - q_{E(complexed)}$. [b] $\Delta q_{cluster} = q_{M_n}(complexed) - q_{M_n}(isolated)$.

to M−O bonds. The $H(r)$'s for Ag−E bonds have the lowest values, when compared to Au−E and Cu−E bonds. It is about 75.0% less than for Au(Cu)−E bonds, and it is in agreement with having the lowest binding energy. (In Table 3, we showed the result of $M_3(t)-EH_2$ complexes.)

Therefore, from the positive values of $\nabla^2\rho(r)$ and negative values of $H(r)$, it can be concluded that M−E bonds must be considered as partially covalent and partially ionic.[42] It should be noticed that the values of $\rho(r)$,$\nabla^2\rho(r)$, and $H(r)$ for the same bonds in different complexes are almost identical.

3.4. Natural Bond Orbital Analysis. ***3.4.1. Natural Population Analysis (NPA).*** NPA was calculated by NBO population analysis. The atomic population of each atom was calculated as the sum of the occupation numbers of all of the natural atomic orbitals (NAOs) corresponding to that atom. In Table 4, charge distributions of the active sites in the complexes are shown. In all of the complexes, interacting metal atoms have a positive charge, and E atoms all have a negative charge. The difference between charges of M and E atoms, Δq_{ME}, ($\Delta q_{ME} = q_{M(complexed)} - q_{X(complexed)}$) for M−O bonds is about 70.0% more than that for M−S(Se) bonds. (This result has been demonstrated by means of QTAIM analysis in section 3.3)

It is evident that the differences of charges in the coinage metal clusters, $\Delta q_{cluster}$ ($\Delta q_{cluster} = q_{M_n}(complexed) - q_{M_n}(isolated)$), are negative, implying that the coinage cluster oxidizes the H_2E molecules. The $\Delta q_{cluster}$ values for gold clusters are about 47.0% more than those for silver and copper ones; therefore, the tendency of gold clusters to oxidize the ligand is more than that for other coinage metals.

3.4.2. Bond Orders and the Polarity of the Bond. Several methods may be used within the NBO formalism to evaluate bond orders.[23,43] The qualitative behavior of bond orders upon delocalization can be rationalized in terms of resonance structures. Resonance weights derived from natural resonance theory (NRT) are used to calculate natural bond order and other atomic and bond indices reflecting the resonance composition of the wave function. The formal bond order between atoms A and B is defined as

$$b_{AB} = \sum_{\alpha} \omega_\alpha b_{AB}^{(\alpha)}$$

where $b_{AB}^{(\alpha)}$ is the (integer) number of bonds in the idealized Lewis-type structural formula for resonance structure α and ω_α is the effective weight of this resonance structure.

A characteristic feature of the NRT treatment is the description of bond polarity by a bond "ionicity index" (resonance-averaged NBO polarization ratio), which replaces the "covalent−ionic resonance" of Pauling−Wheland theory and explicity exhibits the complementary relationship of covalency and electrovalency that underlies empirical assignments of atomic valency.

Fractional ionic character (ionicity index) i_{AB} can be defined as the resonance-weighted average

$$i_{AB} = \frac{\sum_{\alpha} \omega_\alpha i_{AB}^{(\alpha)}}{b_{AB}}$$

where $i_{AB}^{(\alpha)}$ is the corresponding fractional ionic character in resonance structure α, defined from the NBO polarization coefficient. In terms of the fractional ionic character, one can formally partition the total bond order $b_{AB}^{(N)}$ into its "electrovalent" (ionic) and "covalent" contributions, $e_{AB}^{(N)}$ and $c_{AB}^{(N)}$, respectively:

$$e_{AB}^{(N)} = b_{AB}^{(N)} i_{AB}$$

$$c_{AB}^{(N)} = b_{AB}^{(N)}(1 - i_{AB})$$

$$b_{AB}^{(N)} = e_{AB}^{(N)} + c_{AB}^{(N)}$$

Table 5 shows the results of the natural bond orders for M−E bonds (b_{ME}). For these bonds, b_{ME} values have the order of M = Au > Cu > Ag, which agrees with the previous results for M−E binding energies and bond lengths. This table also shows polar covalency and electrovalency of the M−E bonds for $M_3(t)-EH_2$ complexes. Clearly, the Au−S and Au−Se bonds have highest percent of covalency, 27.09 and 31.55%, respectively. Conversely, the M−O bonds have the highest percent of electrovalency and the highest values of charge difference of M and O atoms (Δq_{ME}).

3.4.3. Charge-Transfer Analysis. A useful aspect of the NBO method is that it provides information about the interactions in both filled and virtual orbital spaces that facilitates the analysis of intra- and intermolecular interactions.

A second-order perturbation theory analysis of the Fock matrix was carried out to evaluate the donor−acceptor interaction in the NBO basis. The interactions result in a loss of occupancy from the localized NBOs of the idealized Lewis structure into the empty non-Lewis orbitals. For each donor NBO (i) and acceptor (j), the stabilization energy $E(2)$, associated with the delocalization $i \rightarrow j$ is estimated by

$$E(2) = \Delta E_{ij} = \Delta E_{CT} = -2\frac{\langle i|\hat{F}|j\rangle^2}{\varepsilon_j - \varepsilon_i}$$

where ε_i and ε_j are NBO orbital energies, and $\hat{F}$ is the Fock operator.

The quantities of transferred charge from a given donor orbital to a given acceptor orbital may be estimated again using the perturbation theory arguments, leading to the following approximate formula:

$$q_{CT} \approx 2\left(\frac{\langle i|\hat{F}|j\rangle}{\varepsilon_j - \varepsilon_i}\right)^2$$

As we discussed in section 3.2.3 for M_n-EH_2 complexes, charge transfer from the lone pair of E atoms to the coinage metal atom can be responsible for interaction effects. In Table 6, ΔE_{CT} and q_{CT} for the M−E bonds in $M_3(t)-EH_2$ and $M_4(d)-EH_2$ complexes are listed. For the same metal, the amounts of ΔE_{CT} and q_{CT} have the order of $H_2Se > H_2S > H_2O$. In these cases, charge is transferred from the lone pair of chalcogen atoms to the σ^* and n* orbitals of coinage metal atoms.

By comparing ΔE_{CT} and q_{CT} for $Au_3(t)-EH_2$ complexes, we found that these values for $Au_3(t)-S(Se)H_2$ complexes are about

TABLE 5: Summary of Natural Bond Order and Covalent and Ionic Electrovalent Contributions of the Optimized Structures of M_n-EH_2 Complexes

complex	b_{ME}[a](NRT)		NRT bond order[b]	% covalent	% ionic
$Au_3(t)-OH_2$	0.021	α	0.0155t = 0.0006c + 0.0149i	3.66	96.34
		β	0.0058t = 0.0002c + 0.0056i		
$Au_3(t)-SH_2$	0.332	α	0.1073t = 0.0277c + 0.0796i	27.09	72.91
		β	0.2243t = 0.0636c + 0.1607i		
$Au_3(t)-SeH_2$	0.365	α	0.1424t = 0.0422c + 0.1002i	31.55	68.45
		β	0.2226t = 0.0745c + 0.1481i		
$Ag_3(t)-OH_2$	0.004	α	0.0007t = 0.0000c + 0.0007i	1.52	98.48
		β	0.0033t = 0.0001c + 0.0032i		
$Ag_3(t)-SH_2$	0.007	α	0.0066t = 0.0003c + 0.0063i	2.27	97.73
		β	0.0005t = 0.0000c + 0.0005i		
$Ag_3(t)-SeH_2$	0.013	α	0.0102t = 0.0006c + 0.0097i	4.18	95.82
		β	0.0029t = 0.0001c + 0.0028i		
$Cu_3(t)-OH_2$	0.006	α	0.0035t = 0.0001c + 0.0034i	1.43	98.57
		β	0.0025t = 0.0000c + 0.0025i		
$Cu_3(t)-SH_2$	0.027	α	0.0162t = 0.0006c + 0.0156i	5.17	94.83
		β	0.0105t = 0.0008c + 0.0098i		
$Cu_3(t)-SeH_2$	0.020	α	0.0079t = 0.0004c + 0.0075i	6.77	93.23
		β	0.0118t = 0.0010c + 0.0108i		

[a] b_{ME} = M−E natural bond order. [b] Total (t) NRT bond order is the sum of covalent (c) plus ionic (i) bond order.

TABLE 6: Result of Second-Order Perturbation Theory Analysis of the Fock Matrix within the NBO Basis for Some Selected Complexes

complex	charge transfer	ΔE_{CT}[a]	q_{CT}
$Au_3(t)-OH_2$	$n_{O4} \rightarrow \sigma^*_{Au1-Au3}(\alpha)$	11.99	0.033
	$n_{O4} \rightarrow n^*_{Au1}(\beta)$	11.46	0.038
$Au_3(t)-SH_2$	$n_{S4} \rightarrow n^*_{Au1}(\alpha)$	45.00	0.247
	$n_{S4} \rightarrow n^*_{Au1}(\beta)$	42.52	0.226
$Au_3(t)-SeH_2$	$n_{Se4} \rightarrow n^*_{Au1}(\alpha)$	52.98	0.352
	$n_{Se4} \rightarrow n^*_{Au1}(\beta)$	49.88	0.318
$Ag_3(t)-SH_2$	$n_{S4} \rightarrow \sigma^*_{Ag1-Ag3}(\alpha)$	13.77	0.053
	$n_{S4} \rightarrow n^*_{Ag1}(\beta)$	15.40	0.074
$Cu_3(t)-SH_2$	$n_{S4} \rightarrow \sigma^*_{Cu1-Cu2}(\alpha)$	11.10	0.032
	$n_{S4} \rightarrow \sigma^*_{Cu1-Cu3}(\alpha)$	11.16	0.032
	$n_{S4} \rightarrow n^*_{Cu1}(\beta)$	25.05	0.108
$Au_4(d)-OH_2$	$n_{O5} \rightarrow n^*_{Au3}$	23.54	0.087
$Au_4(d)-SH_2$	$n_{S5} \rightarrow \sigma^*_{Au3-Au4}$	57.64	0.248
$Au_4(d)-SeH_2$	$n_{Se5} \rightarrow \sigma^*_{Au3-Au4}$	63.78	0.308
$Ag_4(d)-SH_2$	$n_{S5} \rightarrow \sigma^*_{Ag3-Ag4}$	24.30	0.097
$Cu_4(d)-SH_2$	$n_{S5} \rightarrow \sigma^*_{Cu3-Cu4}$	35.86	0.124

[a] ΔE_{CT} in kcal mol^{-1}.

75.0 and 86.0% more than those for the $Au_3(t)-OH_2$ complex, respectively. Consequently, it can be understood in terms of the higher ionization potential of H_2O compared to that of H_2S and H_2Se. On the other hand, the values of ΔE_{CT} and q_{CT} for the same chalcogen dihydride have the order of Au > Cu > Ag. For example, in the $Au_4(d)-SH_2$ complex, ΔE_{CT} is about 57.0 and 38.0% more than that in the $Ag_4(d)-SH_2$ and $Cu_4(d)-SH_2$ complexes, respectively. These values confirmed the lower binding energy of silver compared to that for other coinage metals.

4. Conclusion

Interaction of small neutral coinage metal clusters (M_3 and M_4; M = Cu, Ag, Au) with chalcogen dihydrides (H_2E; E = O, S, Se) have been investigated to realize the bonding mechanism in the coinage metal−molecule junctions, which would allow development of a new molecular device.

Geometrical structure, binding energy, and vibrational frequencies of M_n-EH_2 complexes have been calculated using the DFT-B3LYP method. Geometrical data identify that the structure of the molecules did not change significantly before and after interactions.

Interaction energies in these complexes are related to the ionization potential of the lone pair orbital of H_2E (IP_{H2O} > IP_{H2S} > IP_{H2Se}) and relativistic increase of the EA of the coinage metal. Binding energy calculation indicates that the interactions of the silver cluster are significantly lower than those of the copper and gold clusters. On the other hand, interaction of the copper with H_2O is more than gold; although for the $H_2S(Se)$ molecules, the binding energy of gold is higher than copper, but not extensively. Therefore, gold can be substituted by copper in some cases. The tendency of chalcogen dihydrides to interact with the coinage metals has the order of H_2Se > H_2S > H_2O. Accordingly, we can conclude that in M_n-EH_2 complexes, Au−Se is the strongest bond with a binding energy in the range of −17 to −23 kcal mol^{-1}.

QTAIM analysis has been performed to extract the bond critical point properties. It is shown that $\nabla^2\rho(r)$ and $H(r)$ for M−E bonds are positive and negative, respectively, revealing that these bonds are partially ionic and partially covalent.

NPA obtains the difference of charge (Δq_{ME}) for M−E bonds; these values for M−O bonds are about 70.0% more than those for M−S(Se).

Natural bond order has been calculated, and the bond orders for M−E bonds have the ordering $b_{Au-E} > b_{Cu-E} > b_{Ag-E}$. NRT results show the electrovalent and covalent contributions to the bond order. From these results, Au−S and Au−Se bonds have the highest percent of covalency, 27.09 and 31.55%, respectively.

Second-order perturbation analysis has been applied to show the effect of charge transfer in the formation of these complexes. In these bonds, lone pair electrons of oxygen, sulfur, and selenium are partially transferred to the antibonding orbitals of the metal. ΔE_{CT} has been determined, and obviously, they confirmed the trend of binding energies.

References and Notes

(1) Häkkinen, H.; Landman, U. *Phys. Rev. B* **2000**, *62*, R2287.
(2) Sugawara, K.; Sobott, F.; Vakhtin, A. B. *J. Chem. Phys.* **2003**, *118*, 7808.
(3) Pyykkö, P. *Nat Nanotechnol.* **2007**, *2*, 273.
(4) (a) Knickelbein, M. B. *Annu. Rev. Physiol.* **1999**, *50*, 79. (b) Kshirsagar, A.; Ghebriel, H. W. J. *Chem. Phys.* **2007**, *126*, 244705. (c) Fuchs, H.; Krüger, D.; Rousseau, R.; Marx, D.; Parrinello, M. *J. Chem. Phys.* **2001**, *115*, 4776. (d) Pakiari, A. H.; Jamshidi, Z. *J. Phys. Chem. A* **2007**, *111*, 4391.
(5) Majumder, C.; Briere, T. M.; Mizuseki, H.; Kawazoe, Y. *J. Chem. Phys.* **2002**, *117*, 7669.

(6) (a) Bain, C. D.; Whitesides, G. M. *Angew. Chem., Int. Ed. Engl.* **1989**, *28*, 506. (b) Ulman, A. *An Introduction to Ultrathin Organic Films from Langmuir−Blodgett to Self-Assembly*; Academic Press: San Diego, CA, 1991. (c) Ulman, A. *Chem. Rev.* **1996**, *96*, 1533. (d) Delamarche, E.; Michel, B.; Biebuyck, H. A.; Gerber, C. *Adv. Mater.* **1996**, *8*, 719. (e) Krämer, S.; Fuierer, R. R.; Gorman, C. B. *Chem. Rev.* **2003**, *103*, 4367. (f) Love, J. C.; Estroff, L. A.; Kriebel, J. K.; Nuzzo, R. G.; Whitesides, G. M. *Chem. Rev.* **2005**, *105*, 1103.

(7) (a) Aviram, A.; Ratner, M. A. *Molecular Electronics: Science and Technology*; New York Academy of Sciences: New York, 1998. (b) Tour, J. M., *Molecular Electronics: Commercial Insights, Chemistry, DeVices, Architecture and Programming*; World Scientific Pub. Co. Inc.: Singapore, 2003. (c) James, D. K.; Tour, J. M. *Chem. Mater.* **2004**, *16*, 4423. (d) Tao, N. J. *Nat. Nanotechnol.* **2006**, *1*, 173.

(8) (a) Niemeyer, C. M. *Angew. Chem., Int. Ed.* **2001**, *40*, 4128. (b) Katz, E.; Willner, I. *Angew. Chem., Int. Ed.* **2004**, *43*, 6042. (c) Niemeyer, C. M.; Mirkin, C. A. *Nanobiotechnology: Concepts, Applications and Perspectives*; Wiley-VCH: Weinheim, Germany, 2004. (d) Willner, I.; Katz, E. *Bioelectronics: From Theory to Applications*; Wiley-VCH: Weinheim, Germany, 2005.

(9) (a) Majumder, C.; Briere, T. M.; Mizuseki, H.; Kawazoe, Y. *J. Chem. Phys.* **2002**, *117*, 2819. (b) Sellers, H.; Ulman, A.; Shnidman, Y.; Eilers, J. E. *J. Am. Chem. Soc.* **1993**, *115*, 9389. (c) Beardmore, K. M.; Kress, J. D.; Bishop, A. R.; Grønbech-Jenson, N. *Synth. Met.* **1997**, *84*, 317. (d) Ghebriel, H. W.; Kshirsagar, A. *J. Chem. Phys.* **2007**, *126*, 244705. (e) Li, G. P.; Hamilton, I. P. *Chem. Phys. Lett.* **2006**, *420*, 474. (f) Krüger, D.; Fuchs, H.; Rousseau, R.; Marx, D.; Parrinello, M. *J. Chem. Phys.* **2001**, *115*, 4776. (g) Majumder, C.; Kulshreshtha, S. K. *Phys. Rev. B* **2006**, *73*, 155427. (h) Bilić, A.; Reimers, J. R.; Hush, N. S. *J. Chem. Phys.* **2005**, *122*, 094708. (i) Letardi, S.; Cleri, F. *J. Chem. Phys.* **2004**, *120*, 10062.

(10) Ventra, M. D.; Lang, N. D. *Phys. Rev. B* **2001**, *65*, 045402.

(11) Taniguchi, M.; Yokota, K.; Kawai, T. *J. Am. Chem. Soc.* **2007**, *129*, 5818.

(12) (a) Zhou, J.; Li, Z. H.; Wang, W. N.; Fan, K. N. *J. Phys. Chem. A* **2006**, *110*, 7167. (b) Ghanty, T. K. *J. Chem. Phys.* **2006**, *124*, 124304. (c) Konôpka, M.; Rousseau, R.; Štich, I.; Marx, D. *J. Am. Chem. Soc.* **2004**, *126*, 12103. (d) Hsu, W. D.; Ichihashi, M.; Kondow, T.; Sinnott, S. B. *J. Phys. Chem. A* **2007**, *111*, 441.

(13) (a) Antušek, A.; Urban, M.; Sadlej, A. J. *J. Chem. Phys.* **2003**, *119*, 7247. (b) Urban, M.; Sadlej, A. J. *J. Chem. Phys.* **2000**, *112*, 5. (c) Surong, Q. M.; Zhao, Y.; Jing, X.; Li, X.; Su, W. *Int. J. Quantum Chem.* **2004**, *100*, 293.

(14) Konôpka, M.; Rousseau, R.; Štich, I.; Marx, D. *J. Am. Chem. Soc.* **2004**, *126*, 12103.

(15) (a) Schwerdtfeger, P.; Bownmaker, G. A. *J. Chem. Phys.* **1994**, *100*, 4487. (b) Socaciu, L. D.; Hagen, J.; Le Roux, J.; Popolan, D.; Bernhardt, T. M.; Wöste, L.; Vajda, S. *J. Chem. Phys.* **2004**, *120*, 2078.

(16) (a) Stephens, P. J.; Devlin, F. J.; Chabalowski, C. F.; Frisch, M. J. *J. Phys. Chem.* **1994**, *98*, 11623. (b) Becke, A. D. *J. Chem. Phys.* **1993**, *98*, 5648.

(17) Frisch, M. J.; Trucks, G. W.; Schlegel, H. B.; Scuseria, G. E.; Robb, M. A.; Cheeseman, J. R.; Montgomery, J. A., Jr.; Vreven, T.; Kudin, K. N.; Burant, J. C.; Millam, J. M.; Iyengar, S. S.; Tomasi, J.; Barone, V.; Mennucci, B.; Cossi, M.; Scalmani, G.; Rega, N.; Petersson, G. A.; Nakatsuji, H.; Hada, M.; Ehara, M.; Toyota, K.; Fukuda,R.; Hasegawa, J.; Ishida, M.; Nakajima, T.; Honda, Y.; Kitao, O.; Nakai, H.; Klene, M.; Li, X.; Knox, J. E.; Hratchian, H. P.; Cross, J. B.; Adamo, C.; Jaramillo, J.; Gomperts, R.; Stratmann, R. E.; Yazyev, O.; Austin, A. J.; Cammi, R.; Pomelli, C.; Ochterski, J. W.; Ayala, P. Y.; Morokuma, K.; Voth, G. A.; Salvador, P.; Dannenberg, J. J.; Zakrzewski, V. G.; Dapprich, S.; Daniels, A. D.; Strain, M. C.; Farkas, O.; Malick, D. K.; Rabuck, A. D.; Raghavachari, K.; Foresman, J. B.; Ortiz, J. V.; Cui, Q.; Baboul, A. G.; Clifford, S.; Cioslowski, J.; Stefanov, B. B.; Liu, G.; Liashenko, A.; Piskorz, P.; Komaromi, I.; Martin, R. L.; Fox, D. J.; Keith, T.; Al-Laham, M. A.; Peng, C. Y.; Nanayakkara, A.; Challacombe, M.; Gill, P. M. W.; Johnson, B.; Chen, W.; Wong, M. V.; Gonzalez, C.; Pople, J. A. *Gaussian 03*, revision B.04; Gaussian, Inc.: Pittsburgh, PA, 2003.

(18) Peterson, K. A.; Puzzarini, C. *Theor. Chem. Acc.* **2005**, *114*, 283.

(19) Figgen, D.; Rauhut, G.; Dolg, M.; Stoll, H. *Chem. Phys.* **2005**, *311*, 227.

(20) Reed, A. E.; Curtiss, L. A.; Weinhold, F. *Chem. Rev.* **1988**, *88*, 899.

(21) Reed, A. E.; Weinstock, R. B.; Weinhold, F. *J. Chem. Phys.* **1985**, *83*, 735.

(22) Glendening, E. D.; Weinhold, F. *J. Comput. Chem.* **1998**, *19*, 593.

(23) Glendening, E. D.; Weinhold, F. *J. Comput. Chem.* **1998**, *19*, 610.

(24) Glendening, E. D.; Badenhoop, J. K.; Weinhold, F. *J. Comput. Chem.* **1998**, *19*, 628.

(25) Bader, R. F. W. *Atoms in Molecules: A Quantum Theory*; Clarendon: Oxford, U.K., 1990.

(26) Glendening, E. D.; Badenhoop, J. K.; Reed, A. E.; Carpenter, J. E.; Bohmann, J. A.; Morales, C. M.; Weinhold, F. *NBO 5.0*; Theoretical Chemistry Institute, University of Wisconsin: Madison, WI, 2001.

(27) Bader, R. F. W. *AIM2000 Program Package*, version 2.0; McMaster Univeristy: Hamilton, Ontario, 2002.

(28) Bertolus, M.; Brenner, V.; Millie, P. *Eur. Phys. J.* **2000**, *D11*, 387.

(29) L′Hermite, J. M.; Rabilloud, F.; Marcou, L.; Labastie, P. *Eur. Phys. J.* **2001**, *D14*, 323.

(30) Tsipis, A. C.; Tsipis, C. A. *J. Am. Chem. Soc.* **2005**, *127*, 10623.

(31) (a) Balasubramanian, K.; Liao, D. *J. Chem. Phys.* **1991**, *94*, 5233. (b) Balasubramanian, K.; Liao, D. *J. Chem. Phys.* **1992**, *97*, 2548. (c) Zheng, J.; Petty, J. T.; Dickson, R. M. *J. Am. Chem. Soc.* **2003**, *125*, 7780. (d) Lee, H. M.; Ge, M.; Sahu, B. R.; Tarakeshwar, P.; Kim, K. S. *J. Phys. Chem. B* **2003**, *107*, 9994. (e) Soule de Bas, B.; Ford, M. J.; Cortie, M. B. *J. Mol. Struct.: THEOCHEM* **2004**, *686*, 193. (f) Walker, A. V. *J. Chem. Phys.* **2005**, *122*, 094310. (g) Yuan, D. W.; Wang, Y.; Zeng, Z. *J. Chem. Phys.* **2005**, *122*, 114310. (h) Xiao, L.; Wang, L. *Chem. Phys. Lett.* **2004**, *392*, 452. (i) Xiao, L.; Tollberg, B.; Hu, X.; Wang, L. *J. Chem. Phys.* **2006**, *124*, 114309.

(32) Granatier, J.; Urban, M.; Sadlej, A. *J. Phys. Chem. A* **2007**, *111*, 13238.

(33) Powis, I.; Thrower, J. D.; Trofimov, A. B.; Moskovskaya, T. E.; Schirmer, J.; Potts, A. W.; Holland, D. M. P.; Bruhn, F; Karlsson, L. *Chem. Phys.* **2005**, *315*, 121.

(34) Pitarch-Ruiz, J.; Sánchez-Marín, J.; Martín, I.; Velasco, A. M. *J. Phys. Chem. A* **2002**, *106*, 6508.

(35) *CRC Handbook of Chemistry and Physics*; CRC: Boca Raton, FL, 1998.

(36) Pyykkö, P. *Angew. Chem., Int. Ed.* **2004**, *43*, 4412.

(37) (a) Pyykkö, P.; Desclaux, J. P. *Acc. Chem. Res.* **1979**, *12*, 276. (b) Pyykkö, P.; Desclaux, J. P. *Chem. Phys. Lett.* **1976**, *39*, 300. (c) Pyykkö, P. *Chem. Rev.* **1988**, *88*, 563.

(38) Neogrády, P.; Kellö; V.; Urban, M.; Sadlej, A. J. *Int. J. Quantum Chem.* **1997**, *63*, 557.

(39) Hotop, H.; Lineberger, W. C. *J. Phys. Chem. Ref. Data* **1975**, *14*, 731.

(40) Bader, R. F. W. *Chem. Rev.* **1991**, *91*, 893.

(41) Cremer, D.; Kraka, E. *Angew. Chem.* **1984**, *23*, 627.

(42) Bianchi, R.; Gervasio, G.; Marabello, D. *Inorg. Chem.* **2000**, *39*, 2360.

(43) (a) Reed, A. E.; Schleyer, P. v. R. *Inorg. Chem.* **1988**, *27*, 3969. (b) Reed, A. E.; Schleyer, P. v. R. *J. Am. Chem. Soc.* **1990**, *112*, 1434.

JP804033W